Vol. 8 • No. 18 • September 19 • 2019

www.advhealthmat.de

ADVANCED HEALTHCARE MATERIALS

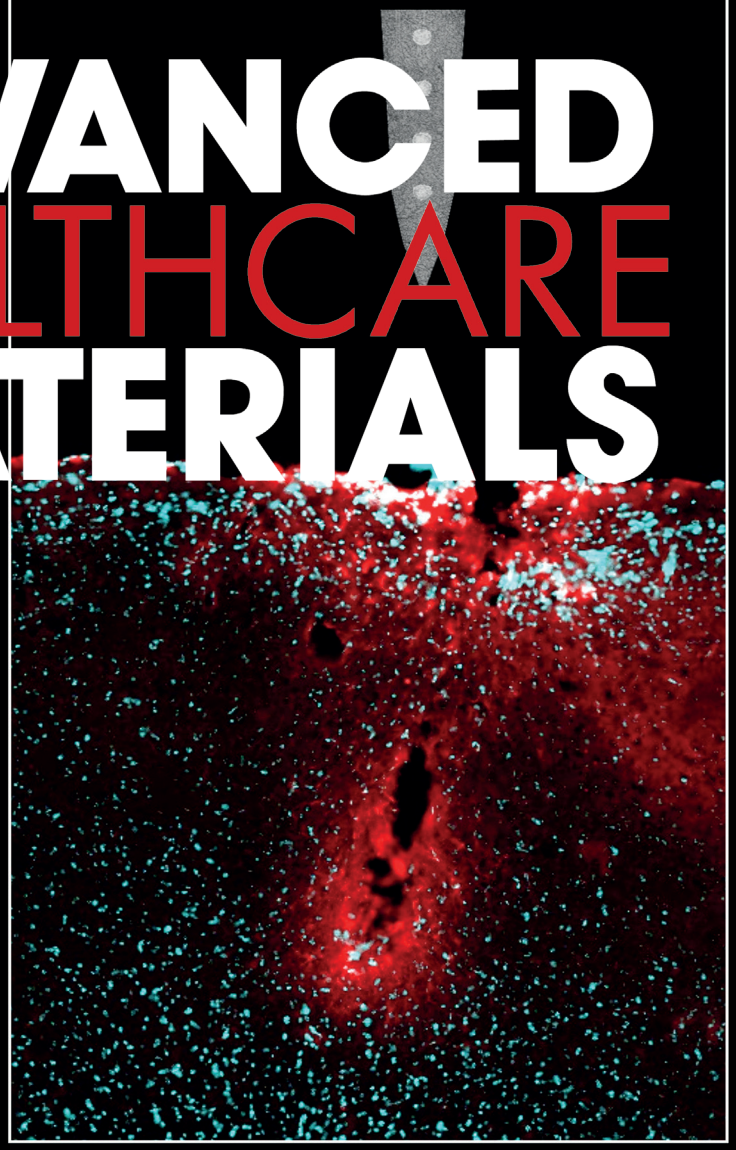

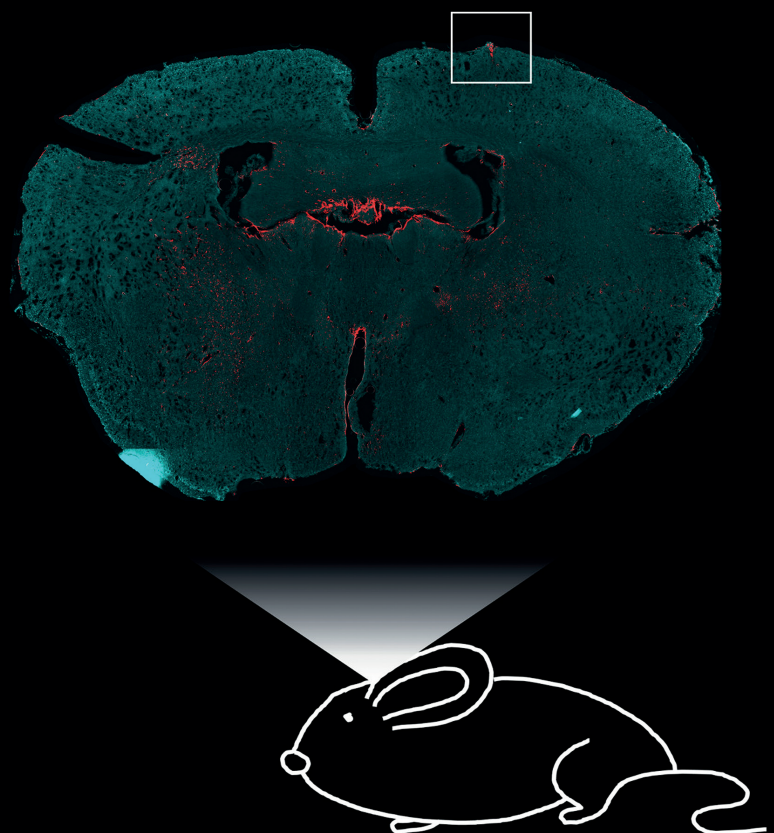

WILEY-VCH

ADVANCED HEALTHCARE MATERIALS
www.advhealthmat.de

Monolayer Graphene Coating of Intracortical Probes for Long-Lasting Neural Activity Monitoring

Antoine Bourrier, Polina Shkorbatova, Marco Bonizzato, Elodie Rey, Quentin Barraud, Gregoire Courtine, Riadh Othmen, Valerie Reita, Vincent Bouchiat, and Cécile Delacour*

The invasiveness of intracortical interfaces currently used today is responsible for the formation of an intense immunoresponse and inflammatory reaction from neural cells and tissues. This leads to a high concentration of reactive glial cells around the implant site, creating a physical barrier between the neurons and the recording channels. Such a rejection of foreign analog interfaces causes neural signals to fade from recordings which become flooded by background noise after few weeks. Despite their invasiveness, those devices are required to track single neuron activity and decode fine sensory or motor commands. Specially, such quantitative and long-lasting recordings of individual neurons are crucial during a long time period (several months) to restore essential functions of the cortex, disrupted after injuries, stroke, or neurodegenerative diseases. To overcome this limitation, graphene and related materials have attracted numerous interests, as they gather in a same material many suitable properties for interfacing living matter, such as an exceptionally high neural affinity, diffusion barrier, and high physical robustness. In this work, the neural affinity of graphene monolayer with numerous materials commonly used in neuroprostheses is compared, and its impact on the performance and durability of intracortical probes is investigated. For that purpose, an innovative coating method to wrap 3D intracortical probes with a continuous monolayer graphene is developed. Experimental evidences demonstrate the positive impact of graphene on the bioacceptance of conventional intracortical probe, in terms of detection efficiency and tissues responses, allowing real-time samplings of motor neurons activity during 5 weeks. Since continuous graphene coatings can easily be implemented on a wide range of 3D surfaces, this study further motivates the use of graphene and related materials as it could significantly contribute to unveil the current rejection of neural probes currently used in many research areas, from fundamental neurosciences to medicine and neuroprostheses.

1. Introduction

Current electroencephalography (EEG) and electrocorticography (ECoG) provide practical tools to monitor whole-brain activity, revealing the role of specific brain regions in various body functions. However, due to overlapping of many different signals it is difficult to extract specific information (such as for accurate movement) which is held by a small number of neurons in the form of single potential spikes. For example, complex hand movements in 3D space or locomotion are generated by the activity of around 50 neurons in the motor cortex.[1–4] Signals from such a small neural population easily vanish within the EEG/ECoG activity and are not detected. For that purpose, penetrating intracortical electrodes that are in direct contact with neurons have been developed, to record with an array of sensors—Utah[5] or Michigan[6] array for instance—multiples spikes generated by several unique motoneuron. Their high spatial resolution is proportional to the electrodes pitch and size, about 400 µm and 50 to 100 µm, respectively. These intracortical microelectrodes were successfully used as brain–machine interface (BMI) in paralyzed patients, allowing them to control prosthetic devices.[7–9]

Although penetrating electrodes were successfully used for movement restoration, their long-term implantation remains a critical issue due to inflammatory and immune responses, which limit their resolution, efficiency, and long-term reliability for chronic recordings.[10–12] Causes of failure are numerous, coming either from the device (e.g., corrosion, delamination of the insulating layer, or electrodes materials, increased tissue impedance) or from the cells and tissues (e.g., disrupted networks during the devices implantation, astrogliosis, and inflammatory reaction).

The strong mismatch that exists between the soft living matter and the inorganic solid-state electronics is also a major limitation because both the chemical contrast and mechanical stiffness impede the efficient and chronic electrical coupling to the targeted neurons.[13] Cells and tissues are order of

A. Bourrier, R. Othmen, V. Reita, V. Bouchiat, C. Delacour
Institut Néel
CNRS and Université Grenoble-Alpes
38042 Grenoble, France
E-mail: cecile.delacour@neel.cnrs.fr
P. Shkorbatova, M. Bonizzato, E. Rey, Q. Barraud, G. Courtine
Center for Neuroprosthetics and Brain Mind Institute
School of Life Sciences
Swiss Federal Institute of Technology (EPFL)
Campus Biotech CH-1202, Geneva, Switzerland
The ORCID identification number(s) for the author(s) of this article can be found under https://doi.org/10.1002/adhm.201801331.

DOI: 10.1002/adhm.201801331

magnitude softer and elastic than the current neural probes, with a Young modulus being around 300 Pa and 0.05–100 GPa, respectively.[14] Therefore, the penetrating electrodes cannot match the deformation of the surrounding cells and tissues, and micromovements of the probe can cause huge cell damage, inflammation, and rejection of the implanted devices.

To overcome this issue, soft, flexible, nontoxic, and bioresorbable electronics have attracted numerous interest for long-lasting recording of the nervous systems with minimal invasiveness while keeping high spatiotemporal resolution.[15–17] In addition to high mechanical compliance with the soft cells, polymeric substrates enable to combine electrical recording/stimulation and local delivery of chemical compounds (e.g., drug, growth factor) using fluidic microchannels to support further the healing process of the damaged neuron networks around the implant.[18,19]

Regarding the electrodes design and material, the use of graphene could further overcome several limitations of current neural probes, as it combines in same and single material many suitable features for interfacing living matter, such as high neuronal affinity, chemical inertness, diffusion barrier for chemicals, antioxidation, and anticorrosive properties, optical and magnetic (MRI) transparency, and flexibility while remaining highly conductive. High quality macroscale monolayer graphene sheets can be obtained by chemical vapor deposition (CVD) growth and then transferred onto a wide range of substrates, including soft and stretchable polymeric materials, to keep an intimate coupling with the cells and to further improve the time stability of the implanted devices. Recently, Lu et al.[20] implemented graphene-based microelectrode arrays on flexible polyimide substrate for cortical stimulation and sensing. Also, Park et al.[21] demonstrated the successful association of transparent graphene micro-EcoG with optical imaging and optogenetic activation to monitor neuronal activity in hippocampal slices and animals. Finaly, the graphene field effect transistors (G-FET) technology was successfully applied for recordings sensory-evoked responses on the visual and auditory cortices, and synchronous activity in a rat model of epilepsy.[22] The developed technology provides alternative to the current EEG/EcoG for reducing the electrode size and thus the spatial resolution while reaching state-of-the-art sensing performance (e.g., in terms of signal-to-noise ratio SNR). While further developments are required for interfacing deeper brain regions below the dura mater, these pioneering experiments have paved the road for intracortical graphene neuroelectronics.

Another key advantage of graphene in the race for biocompatible materials could definitely be to support the regeneration of the damaged target neurons instead of the proliferation of reactive astrocytes, which limits the efficiency and the lifetime of implanted devices. Since few years, many studies have reported on the high biocompatibility of this carbon-based material. For instance, it was shown that graphene monolayer supports neuronal attachment and sprouting,[23–26] and increases the stem cell differentiation into neurons.[27,28]

Here, we have compared the impact of graphene on the regrowth of cultured neurons in-vitro with other materials used in neuroprostheses, and regarding the positive feedback provided by graphene we have then investigated the response of cells and tissues to similar graphene coatings in-vivo and its impact on the detection efficiency and time reliability of intracortical electrodes (Michigan type). Without graphene coatings, these rigid neural probes face a strong immune response.[29–31]

2. Results

Graphene biocompatibility assessments within primary neuron culture—first, we have assessed the neural affinity of several substrates compounds currently used as neural interfaces material (silica, nanocrystalline CVD diamond, Parylene-C, Polyimide (PID)) in terms of neurons adhesion and neurites spreading, and compared those substrates with high quality monolayer graphene transferred on glass (see the Experimental Section). Conventional glass coverslips were used as control substrates. Parylene-C and polyimide are often used as insulating materials and flexible substrates for biosensor arrays. For this study both polymer types were deposited onto glass coverslips, as for the graphene monolayer. Half of each sample batches were coated with poly-L-lysine (PLL, a polymer promoting neurons adhesion and outgrowth—commonly used for cell cultures, while the other half remained pristine (bare uncoated polymer). Using the previously described protocol (see the Experimental Section), primary E16 mouse hippocampal neurons were cultured on both coated and pristine substrates. Two samples of each batch were fixed and immunostained at DIV1, 2, 4, and 5. Since at DIV4 and 5, the neural architecture becomes very complex, the main growth characteristics, such as neurite number and neurite length, were compared only at the early growth stage, i.e., at DIV2.

Figure 1 shows representative immunofluorescent micrographs obtained on the different growth substrates after 2 d of culture. While with a PLL coating, all substrates exhibit neural attachment with expected shape and neurite outgrowth, without PLL neurons attach only on graphene. Already at DIV2, neurons start to develop axons, as shown by emerging tau staining (red), which labels the axon-specific microtubules. However, neurons grown on coated glass coverslips exhibit less axon polarization than those cultured on other substrates, including pristine (uncoated) graphene.

The statistical analysis (**Figure 2**) compares the cell density, as well as the neurite number, total outgrowth, and the length of the longest neurite per neuron which is presumably the future axon. The neurons are seeded with the same initial density (124 neurons per mm^2) on all growth substrates, but not all of these neurons attach to the substrate surface. For coated samples, around 66% of seeded neurons are found attached on the diamond surface, while only 42% are attached to the polyimide (PID, as shown in Figure 2a. The low amount of neurons attached to PID could be caused by its higher hydrophobicity—observed prior to PLL deposition—which could affect the homogeneity of the PLL coating. At DIV2, the neuron density decreases for all substrates by around 10–15%. More interestingly, the neural adhesion on pristine graphene (without PLL coating) is significantly higher than for PLL coated substrates, while on noncoated glass, diamond, parylene, and PID statistically no neurons adhere (less than five on the entire sample with substrate diameter of 12 mm).

Neurons—grown on all investigated substrates—exhibit healthy shape and outgrowth. At DIV2, on all PLL coated

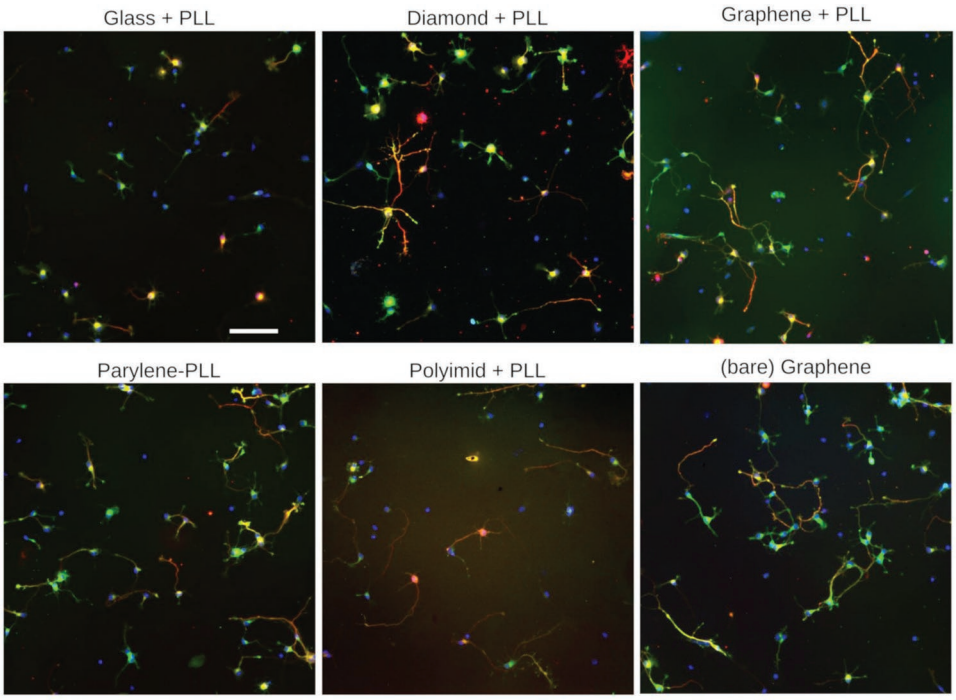

Figure 1. Neural adhesion and growth on different materials used for brain interfacing. Representative immunofluorescent micrographs of 2 d old neurons grown on different substrates (glass, Diamond, parylene, polyimide, and graphene) used in neuroprostheses. In absence of Poly-L-lysine (PLL) neurons only attach and grow on graphene. IF labeling: DAPI (blue) labels the soma, synapsin (green) the synaptic vesicles, and tau (red) the axon. Scale bar is 100 µm.

samples neurons develop in average four neurites, and significantly less than four on pristine graphene (Figure 2b). At this development stage, the initiating axonal polarization can be observed on all growth substrates. However, neurons developing axons are less frequently observed on glass coverslips compared to all other samples. While the number of neurites is statistically equivalent on all coated samples, significant differences were found in terms of the neurite length.

Graphene as well as parylene and PID substrates provide a better stimulation of neurites growth compared to glass control

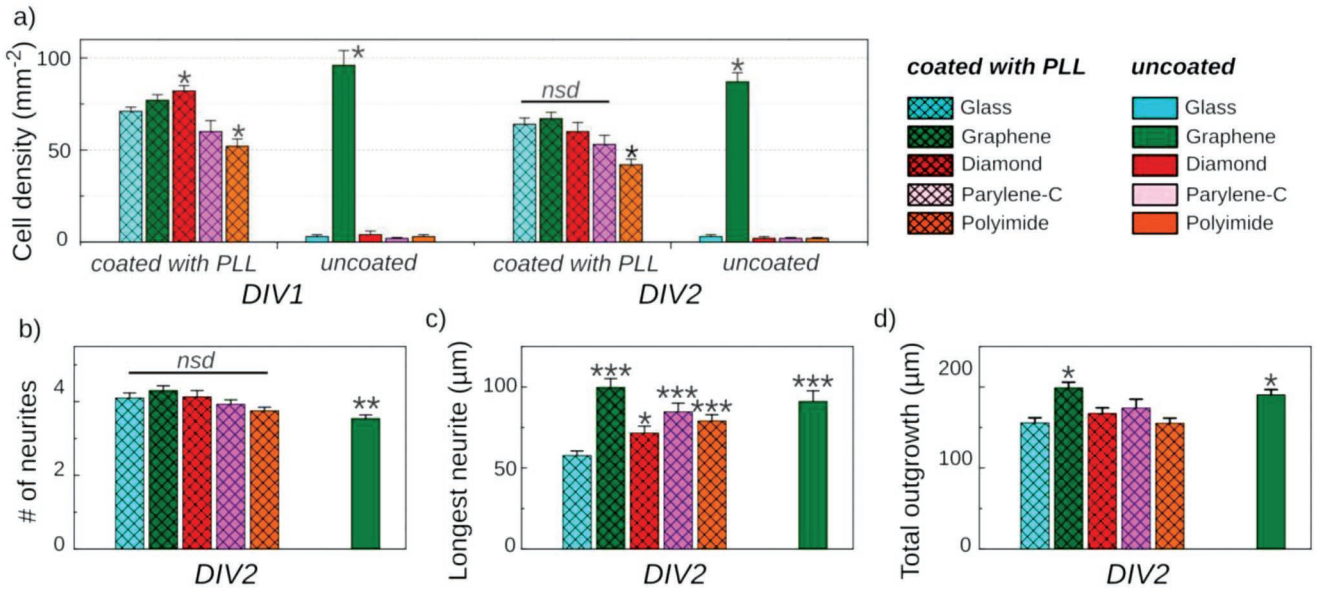

Figure 2. Statistical analysis of the cell culture assays. a) Cell density, b) number of neurites, c) length of the longest neurite presumably the axon, and d) the total outgrowth per neuron in the early development stage (DIV1–DIV2). The results are obtained from one culture with two samples per batch and expressed as mean values ± SEM (with at least 140 neuron per condition). The results were statistically compared to the control PLL coated glass coverslip using ANOVA followed by Bonferroni test with significance levels: $*p < 0.05$, $**p < 0.005$, and $***p < 0.001$, "nsd" means no significant difference.

samples. As shown in Figure 2c, the neurons cultured on these substrates exhibit significantly higher length of the longest neurite per neuron than those grown on glass coverslips, which reflects the less frequently observed axonal polarization. As already mentioned above, the neurite outgrowth strongly depends on the stiffness of the growth substrate.[32] During their development the neurons continuously probe the surrounding environment via neural growth cones, which are highly motile structures at the neurite ends. These cones are capable of recognition and controlled response to the mechanical/chemical properties of the growth substrate.[33] For example, it was shown that neurons retract and re-extend their processes in response to the increased stiffness.[34] As a result, the axonal elongation is delayed on stiff substrates, such as glass coverslips and diamond, and accelerated on soft materials, such as parylene and PID. PLL-coated diamond exhibits slightly higher maximal neurite length, than control glass coverslip, which can be attributed to the increased substrate roughness.[35] Neurons grown on PLL coated and pristine graphene develop the longest maximal neurites.

Despite the significant differences in the maximal neurite length, the total outgrowth, calculated as the cumulative length of all neurites emerging from the same soma, is statistically equivalent on all coated substrates, except graphene (Figure 2d). Again, this observation reflects the accelerated axonal differentiation on soft polymers and diamond. The mass gain/total growth velocity of the neurons seems to be preserved on all substrates: while on glass coverslips all neurites grow almost equally fast, on polymers and NCD the dendrite growth is delayed to benefit the earlier axonal polarization. Graphene however seems to actively promote the neural growth. Neurons grown on graphene not only exhibit the longest maximal neurite, but also the highest total outgrowth, revealing that graphene accelerates all processes in the neurons regrowth. More importantly, neurons grown on pristine graphene exhibit similar amount of processes as those grown on PLL-coated graphene, and higher total outgrowth than those cultured on other coated substrates.

Unlike other substrates, graphene significantly improves the neuronal growth even without an adhesive coating, revealing its exceptionally high neural affinity. Hence, using graphene coatings could significantly improve the viability and connectivity of neural networks while providing a detection port through its electrical conductivity and charge sensitivity. Also, the physical stability and flexibility of graphene together with the possibility to bypass the protein coating reveal its great potential for neuroprostheses.

Impact of graphene on the acceptance of intracortical neural probes—starting from these previous observations, we have investigated the impact of pristine graphene on intracortical probes, in terms of cell and tissues responses and electrodes connection reliability and time stability. To do so, we have wrapped Michigan-type silicon probes (Q-trode, from Neuronexus) with a graphene monolayer as described in **Figure 3**a,b (also detailed in Experimental Section). The free-carrier transfer method that we report was adapted from previous studies which have shown, for instance, the ability to transfer monolayer graphene on unconventional substrates[36] and the mechanical robustness of free-standing graphene based devices such as graphene kirigami.[37] As expected from those previous studies, the results that we obtained are highly reproducible and have been assessed on numerous samples (8 commercial probes, 5 for in-vivo assays and 3 for ex-vivo characterizations, and about 20 home-made silicon probes were also used for preliminary tests). The quality of the transfer was assessed by multiple analysis including optical and electronic (SEM) microscopies, Micro-Raman mapping and electrical measurement of graphene sheet resistance. Typical Raman spectra (Figure 3c) and Raman mapping of the 2D band and G band intensity (I_{2D}) and (I_G) confirm the presence of graphene above the recording sites (Figure 3d,e) and between electrodes (Figure 3f). Also, representative scanning electron micrographs (Figure 3g,h) illustrate the final silicon probe wrapped with the graphene monolayer which is clearly revealed by the presence of wrinkles and multilayer patches (underlined by the arrows). This series of Raman maps and SEM micrographs demonstrate the homogeneous coating of the probe with the monolayer graphene, including the recording channels carried by each silicon probes, the electrode size and pitch being around 25 and 50 µm respectively (additional SEM micrographs are provided in Figure S3 of the Supporting Information). As shown by Raman spectroscopy (Figure 3c), the quality of the graphene monolayer after the wet transfer appears slightly depressed compared with monolayers transferred with a PMMA-carrier on 2D flat surfaces,[26] with the appearance of the disorder-induced D band peak ($w_D \approx 1350\ cm^{-1}$) and the D' band peak observed as a shoulder of the G peak.[38] Also the intensity of the G-band peak ($I_G/I_{2D} \approx 0.8$) and the shift of the 2D peak ($\Delta w_{2D} \approx 2700\ cm^{-1}$) are characteristics of multilayer graphene. These features are induced by the numerous wrinkles observed on the several SEM micrographs (Figure 3; Figure S3, Supporting Information) that increase the Raman defect-related-peak intensity (D-band) and the I_G/I_{2D} intensity ratio. The high density of wrinkles results from the absence of the PMMA resist, commonly used to transfer graphene (see the Experimental Section). The resist carrier contributes indeed to stretch and flatten the graphene layer over the substrate, preventing the formation of additional wrinkles (Figure S4, Supporting Information). At the opposite, more wrinkles are observed on the SEM micrographs (Figure 3g,h) when transferring pristine monolayer graphene without resist carrier. Nevertheless, the material is still high crystalline quality graphene, with the presence of mono and bilayers generated at the wrinkles.[38] This method is the only way to coat uniformly a 3D probe with graphene without leaving any potential cytotoxic component like resist residual on the surface.

A crossview scheme of the graphene-coated IrO*x* electrode is described within **Figure 4**a. The average resistance measured between two electrodes sites is more than an order of magnitude higher than each individual electrode's impedance toward the medium (Figure 4b). Consequently, the total impedance is dominated by the electrode–electrolyte impedance (about 0.3 MΩ at 1 kHz) rather than the electrode-to-electrode resistance (above the GΩ range) and short-circuit path between electrodes is rather negligible. As depicted in Figure 4a, the graphene monolayer is expected to tear apart along the 200 nm high step induced at the insulating SiO_2/IrO*x* interface due to the high attractive interaction with the substrate, which confirms the strong adhesion of graphene over the surface including at the sensing sites.

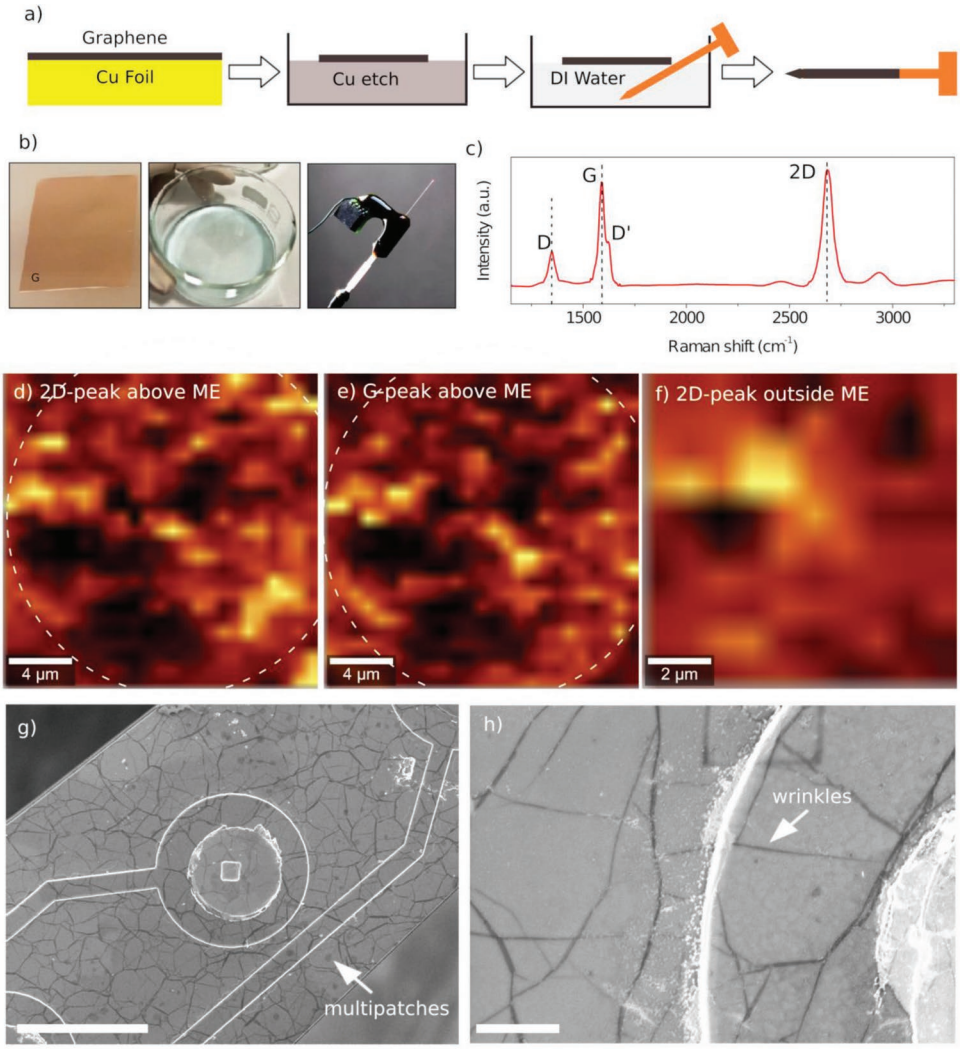

Figure 3. Graphene-coating of 3D intracortical neural probe. a) Schematic method for the wet transfer of graphene on 3D intracortical implant. b) Optical pictures show the monolayer at several steps of the process, from left to right: on Cu foil, in DI water before the fishing, and the final neural probe. c) Representative Raman spectrum performed above the recording sites (4 channels per probe, as shown in g) with the characteristic Raman peaks of monolayer graphene. d–f) Raman mapping of the 2D band and G band intensity (I_{2D}) and (I_G) above the recording site (d and e, respectively, and between adjacent electrodes f) confirming the presence of graphene over the IrOx electrodes. g,h) SEM micrographs of the probe coated with graphene and close view at the SiO_2/IrOx interface (as depicted in Figure 4a) showing the homogeneous Gr-coating of the recording channels. The several wrinkles and multipatches (underlines by arrows) reveal the presence of graphene all over the tip. Scale bars 20 and 2 µm.

Few devices, for which the graphene has not been broken and remained continuous at the SiO_2/IrO*x* step, have been followed before and after the implantation surgery (see the Discussion Section). These persistent connections allowed us to assess the presence of a continuous layer of graphene after the penetration of the implant through the cortical layers. The square resistance of the graphene monolayer, measured between those recording sites, is around $R_{\square} = 0.7 - 1\ \text{k}\Omega\ \square^{-1}$. This is slightly higher than the usual value for high quality graphene transferred with resist carrier on flat substrate ($R_{\square} = 0.65 \pm 0.05\ \Omega_{\square}^{-1}$),[39] but it confirms the continuity of the monolayer after its implantation.

Electrochemical impedance spectroscopy (EIS) measurements were performed on graphene coated IrO*x* electrodes in PBS, over the frequency range from 10 Hz to 0.1 MHz, with 50 mV modulation amplitude (Figure 4c). The magnitude (upper panel) and the phase (lower panel) of the impedance of the electrode–electrolyte interface are as expected for IrO*x* microelectrodes.[40] Although the graphene coating seems to slightly enhance the impedance values (as shown within Figure 4b at 1 kHz, adding one graphene monolayer does not significantly change the Bode diagram of the electrode. Cyclic voltammograms of the bare and graphene-coated electrodes have been recorded at 0.1 V s^{-1} in PBS (Figure 4c). The leakage current between the electrode and the electrolyte is about few nA, and remains almost at the same amplitude for the two tested conditions, with and without graphene coating (lower and upper panel of Figure 4c, respectively). As expected, graphene does not significantly alter the out-off plane transport properties of the electrode–electrolyte interface, regarding the low quantity of inserted material (only one single atomic layer).

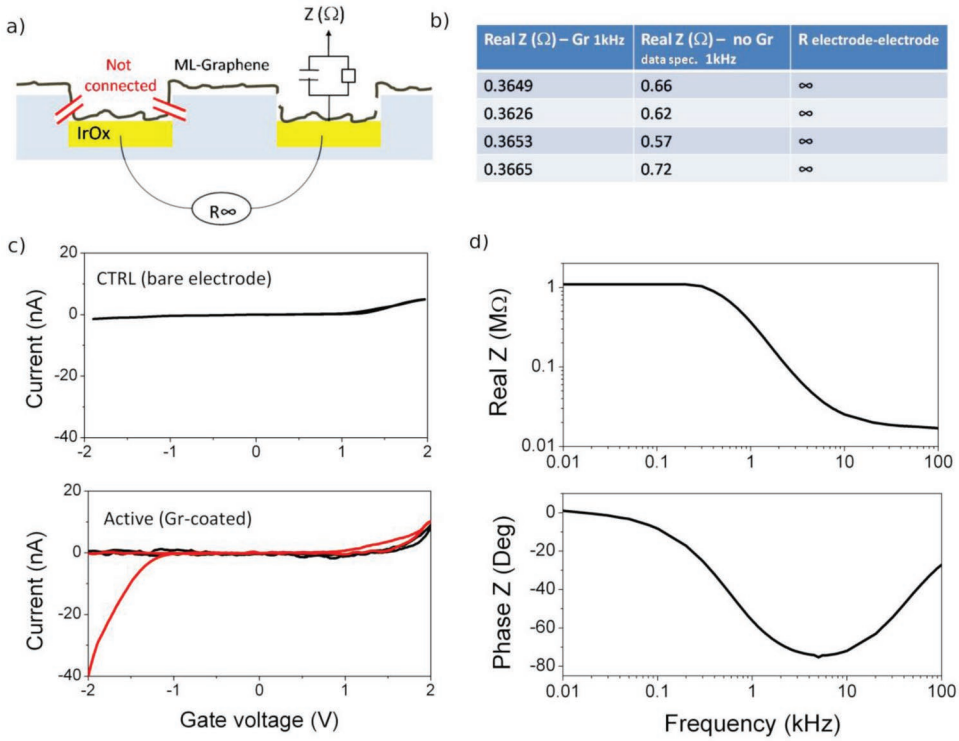

Real Z (Ω) – Gr 1kHz	Real Z (Ω) – no Gr data spec. 1kHz	R electrode-electrode
0.3649	0.66	∞
0.3626	0.62	∞
0.3653	0.57	∞
0.3665	0.72	∞

Figure 4. Electrochemical characterization of graphene coated electrodes. a) Schematic picture of the recording channel (IrOx electrode) embedded in SiO_2 insulating layer (excepted at the recording site) and covered by a monolayer graphene. b) The impedance with the liquid media (PBS) at 1kHz and the resistance between adjacent electrodes, measured with and without graphene. c) Electrochemical impedance spectroscopy and d) cyclic voltammograms performed on graphene-coated IrOx electrodes in PBS, show that the electrodes impedance and charge storage capacity remain almost the same (same order of magnitude) with and without graphene. The impendence values are reported in b) at 1kHz without graphene.

Ten probes from the same commercial batch were used and splitted into two sub-batches (5 probes coated with graphene, 5 bare control probes providing 40 recording channels in total, and 20 for each condition with/without graphene) and were inserted in the motor cortex of rodents. In order to trigger lower limb movement on demand and thus better synchronize recordings with locomotion, transgenic mice were chosen to express ChRod in their motorcortex and thus be sensitive to optical stimulation according to previously described protocol.[41] Briefly, mice were anesthetized with Dorbene and kept unconscious with isofluorane gas while a stereotaxic frame helped maintaining the head during the probe insertion, performed under a binocular to control eventual bleeding. All probes are connected to zero-insertion-force connector for in-vivo recordings, and compared with control (uncoated) probes. Signals are recorded and amplified (TDT-PZ2 preamp and RZ2 amplifier) at the sampling rate of about 25 kHz. Spike sorting is processed in real-time by using (TdT OpenEx) commercial software and spikes of interest are stored, i.e., when spike occurrence matches with the walking status. Optical stimulations—performed with the optical fiber integrated on same probe (red spot at the apex of the probe in Figure 3b)—allowed to activate and to identify the recorded motor neurons. For each probes and electrodes, the experience was repeated weekly by in-cage free-movement recordings.

The detection efficiency of the electrodes is monitored as a function of time, and compared in terms of amplitude, duration, and number of detected spikes. **Figure 5**a shows typical neural spikes associated to walk status. One can clearly distinguish three different shapes of spike that correspond to three distinct motor neurons (Figure 5b). The amplitude (550 μV), duration (1–2 ms), and polarity of the detected extracellular spikes are those expected for motor neurons regarding previously reported values within rodent neocortex detected with similar microelectrode arrays,[42] with peak-to-peak to noise ratios (SNR ≈ 6) being significantly higher than four standard deviations of the background.

To assess for the time reliability of the recordings for the two types of coatings (graphene coated vs uncoated control electrodes), we have tracked this recording quality in terms of signal to noise ratio and spike shape for each mouse and each microelectrode (4 microelectrodes per probe and per mouse, 40 electrodes tested in total, 20 microelectrodes coated with graphene, and 20 uncoated control microelectrodes). Typically, we counted the number of sensors that enable the detection of a single unit emitted from motor neurons with same recording quality (e.g., in terms of amplitude, SNR, duration, polarity) as shown in Figure 5b, as function of the time. After 3 weeks of implantation, the graphene-coated electrodes are capable of recording motor neuron activity with a mean-operational rate of 50%, while the number of operational control (uncoated) microelectrodes strongly decreases with a mean operational rate of around 10%. At 5 weeks, less than 25% of control electrodes remain functional which is the minimum value reached

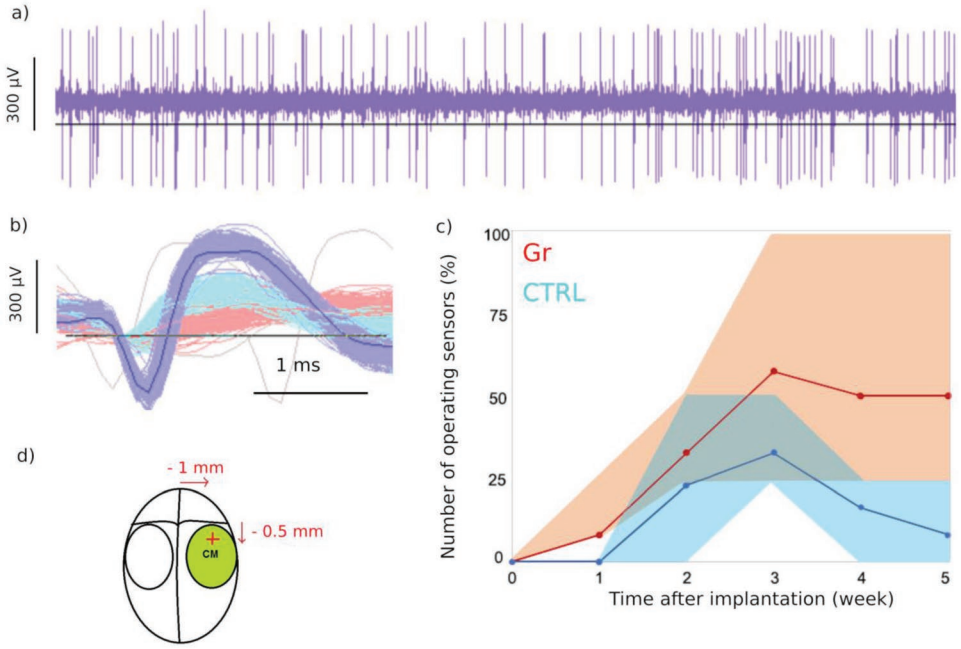

Figure 5. Impact of graphene on the detection efficiency of intracortical probes. a) Representative voltage time trace of the graphene-coated NeuroNexus probe. b) Superimposed detected spikes extracted from a) showing three distinguishable shapes (amplitude, duration, firing rate, each being associated to one individual neuron. c) Detection efficiency over the implantation time (5 weeks) for the graphene-coated probes (red, compared to control (uncoated) samples (blue, giving the average number of operational electrodes (bold line) and the maximum deviation from the mean value (large line) for each experimental condition. d) Schematic illustration of the implanted location over the mouse brain in-plan view.

with the graphene-coated probes that can achieve 100% of efficiency even after 5 weeks of implantation, meaning that all electrodes per coated probe enable the detection of single spike associated to the walk status. Few studies have assessed the time reliability of similar silicon probes which show uneven success. Most have reported failure to achieve stable recordings with reasonable signal to noise ratio. For instance, L. Karumbaiah et al.[29] showed that almost all channels exhibit an SNR below the detection threshold preventing single unit detection after 10 d. Other groups were more successful,[30] but still they reported low rate of operational sensors able to detect single unit (50–25%) and weak single-to-noise ratio (around SNR = 2 first, and rapidly declining around SNR = 1 after few weeks). These previous reports agree with our observations regarding the control (uncoated) silicon probes, the maximum value of operational sensors being about 25% after the scaring process, and rapidly decreasing after few weeks. The results obtained with the graphene-coated probe demonstrated a signal quality and durability enhancements of the neural probes reliability, suggesting improvements either of the surface electrode bioacceptance, or of the electrical coupling to neurons.

To further investigate these apparent improvements induced by the graphene coating in terms of signal quality and time reliability, we characterized the cell and tissues response around the implant by postmortem immunohistochemistry. At the end of the recording procedures (5 weeks after implantation, brains were dissected, fixed, and immunostained. Fifty-five 55 coronal sections slices (30 µm thick) were incubated with anti-Iba1 and anti-GFAP primary antibodies to label the microglia and the astrocytes, which usually proliferate around foreign implanted interface.[10] The soma and neurites are labeled using DAPI and Nissl markers, respectively (Experimental Section). The thin slices were then observed with a confocal fluorescence microscope to estimate the glial cells population and neurons density around the implanted. **Figures 6** and **7** provide representative fluorescent micrographs showing the density of astrocytes and microglia, respectively, at the implant site, for the two experimental conditions (control and graphene-coated probes). The whole coronal section is provided in Supporting Information for 6 probes (Figure S1, Supporting Information). The density of astrocytes and microglia are significantly reduced around the implanted probes coated with graphene, in comparison to the control probes (statistical analysis shown in Figure S2 of the Supporting Information). At the same time, the surrounding neuron network appears also healthier, with a higher number of soma and neurites around the active implant. At the opposite, the control probes are surrounded by a thick layer of astrocytes and microglia after 5 weeks (Figure 6a), which is indeed as expected for Michigan-style array.[43] The formation of this thick layer of glial cells, being about 100–200 µm, is the probable cause of the signal loss. It is indeed barely possible to envisage reliable detection of single action potentials at distances greater than 100 µm. The proliferation of astrocytes is significantly reduced around the graphene-coated probes (Figure 6b), being around few 10 µm wide (black line, Figure 6c). The network of neurons is also denser and appeared healthier at the probe location (indicated by an arrow within Figure 6d). A similar trend is observed for the microglia, whose density is significantly less, spreading over few microns only from the implant location (Figure 7c). The neurites spreading seems also slightly enhanced around the graphene-coated probe (Figure 7d, black line).

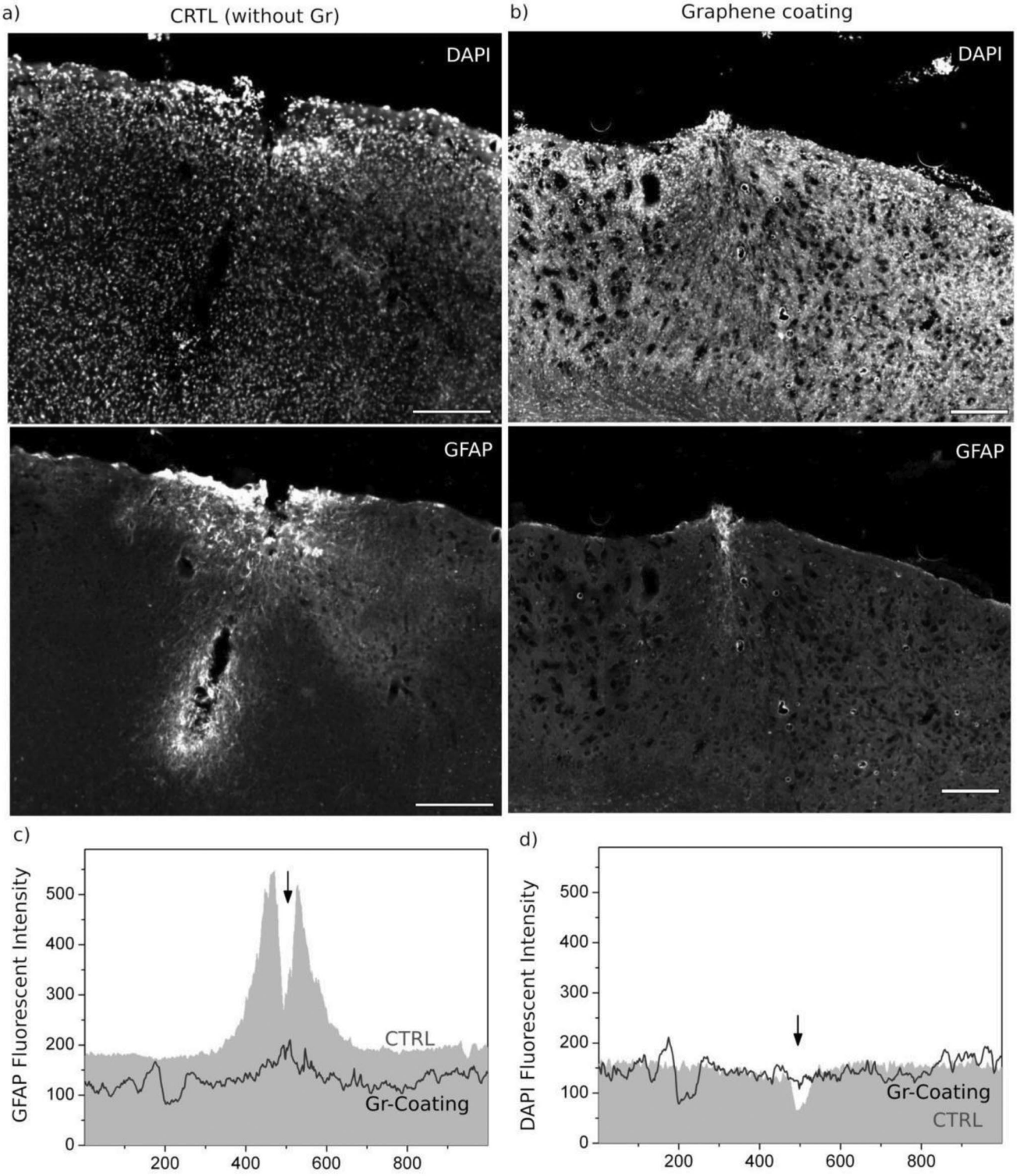

Figure 6. Impact of the graphene coating on the neuron and astrocyte densities around the implant. a) Representative postmortem immunofluorescent micrographs of the tissues fixed and stained after the recordings at 5 weeks (see the Experimental Section), for the uncoated (control) probe a) and for same probe coated with graphene monolayer b). Neuron somas and astrocytes are labeled with DAPI and GFAP antibodies. Scale bar 200 μm. b) Fluorescent intensity profiles revealing the density of astrocytes c) and neurons d) for the control (uncoated) and the graphene coated probes (gray histogram and black line, respectively). The values are averaged over a representative penetration depth around the implant (about 300–500 μm).

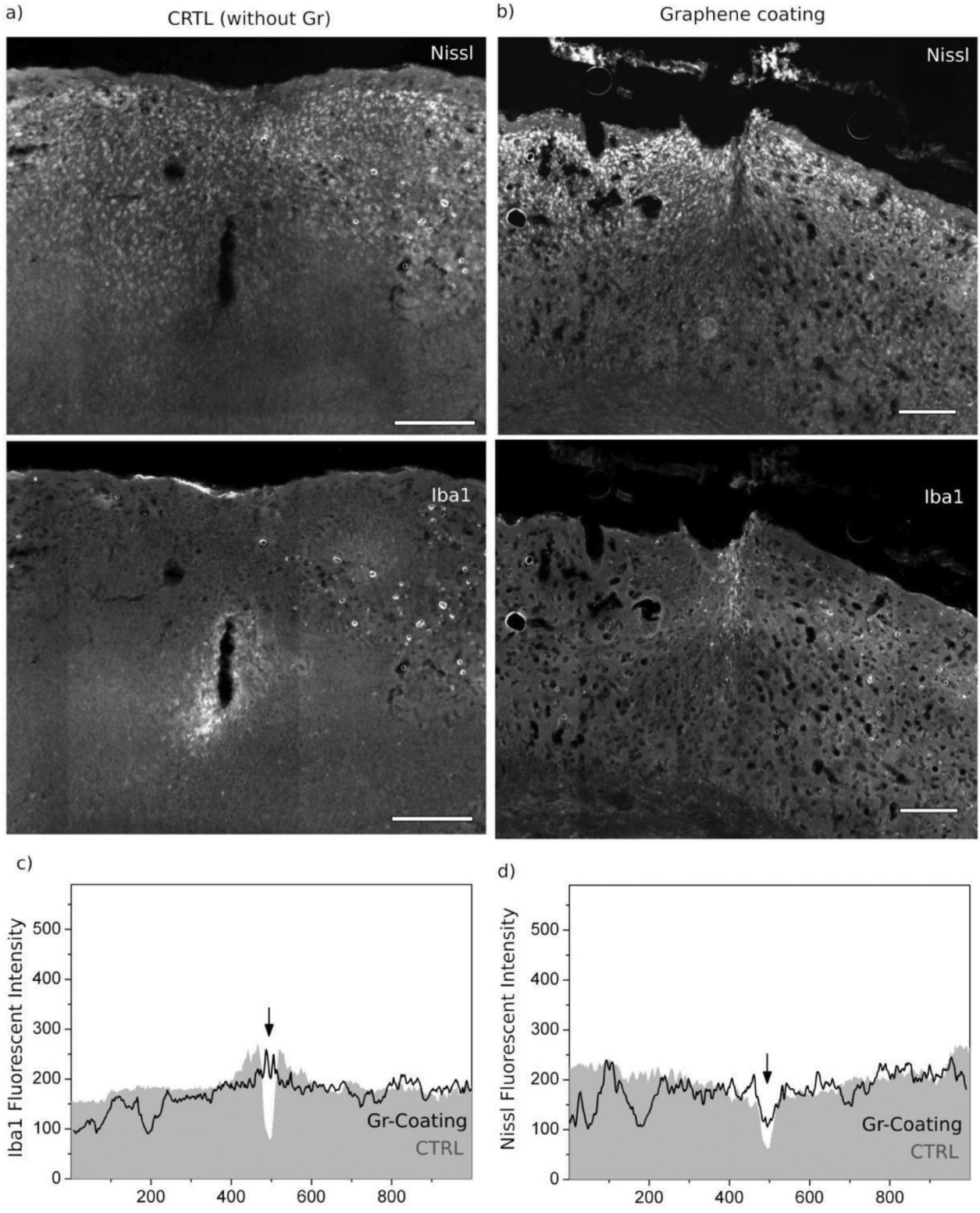

Figure 7. Impact of the graphene coating on neurites and microglia organization around the implant. a) Representative postmortem immunofluorescent micrographs of the tissues fixed and stained after the recordings at 5 weeks (see the Experimental Section), for the uncoated (control) probe a) and for the same probe coated with graphene monolayer b). Neurites and microglia are labeled with Nissl and Iba1 antibodies, respectively (the Experimental Section). Scale bar 200 µm. b) Corresponding fluorescent intensity profiles for each marker Iba1 c) and Nissl d) labeling the microglial and neurites, respectively, extracted from a) and b) to compare the control (uncoated) and the graphene-coated probes (gray histogram and black line, respectively). The values are averaged over a representative penetration depth around the implant (about 300–500 µm).

These results suggest that the enhanced lasting of the intracortical implants coated with graphene are associated with a reduced proliferation of astrocytes and microglia, which allows to keep the intimate coupling between the electrodes and the target neurons and thus supports efficient and reliable recordings.

3. Discussion

The acceptance of intracortical implant is crucial for neurorehabilitation projects because reliable and long-lasting monitorings of single units in freely moving environment are required for replacing disable node of the neural network, and restore sensory function or fine motor command. Such an invasive procedure cannot be repeated as it causes permanent damages to the Brain, thus it is mandatory to improve the chronic acceptance of the current probes for clinical applications. Many strategies have been identified to counterpart the foreign body response,[44] such as reducing the inflammatory reaction by using soft or flexible materials, improving the surface affinity, lowering the materials diffusion out of the implants, or preventing micromotions.[45] Here, we have further investigated how the material in direct contact with the cells and tissues can significantly impact the immune reaction, i.e., the proliferation of reactive astrocytes and microglia around the foreign probe that prevent a close contact with the targeted neurons and thus reliable single spike detection. Because graphene was shown to promote the neuritogenesis in-vitro within numerous neural cell cultures, including ours, we have investigated if a simple monolayer graphene coating could improve the coupling to neuron within intracortical layers in-vivo and be useful to reduce the gliosis.

The expected footprint of conventional Michigan-type neural probe can be clearly observed on our immunohistological analyses (black region Figures 6 and 7, revealing a significant reduction of neurons density at the probe location, which is surrounded by a high density of astrocytes and microglia spreading over 100 µm from the implant site. However, the network of neuron has appeared significantly more preserved when coating the same probe with a monolayer graphene, as we found a higher density of soma and a reduced density of reactive astrocyte around the implant site. The density of microglia also decreased, confirming the reduced immunoreaction around the graphene-coated probe. These observations are in the frame of our previous results obtained in-vitro, showing that monolayer graphene enhanced neurite regrowth in comparison with other materials, and specially silicate glass control samples.

While the mechanisms that sustain the neuritogenesis and neurons adhesion are unclear, many studies have indeed reported the significant improvement gained when using monolayer graphene. For instance, Lee et al.[25] have reported that neurite growth (SH-SY5Y neuroblastoma) may be mediated through FAK and MAPK cascades, and Li et al.[24] showed that Growth-Associated Protein 43 (GAP-43) expression was enhanced in neurons cultured on graphene. FAK, MAPK, and GAP43 are indeed involved in neural cells adhesion and connection to the actin cytoskeleton.[46] Other studies suggested the role of nanotopographical cues within the monolayer that might upregulate neuronal markers,[47] or shown a significant impact of graphene coating in the upregulation of early neurogenesis-related genes.[28] In our study, we have previously shown[26] that CVD-grown graphene combines both positive and stretched surface which are indeed two crucial features sustaining neural outgrowth, and that poor crystalline quality could significantly impede the neural adhesion and growth. Graphene also offers a flexibility at the cell scale compared to rigid substrate which could also play a significant role in the neurite sprouting and cell motility,[48] in addition to other biosuitable properties of graphene, such as nanoscale structure, robust, mechanically deformable, electrical conductivity, and absorption of biomolecules.[49] This unique combination gathered in a single material can indeed collectively support the neurons regrowth and improve the acceptance of the foreign interface. Further investigations would contribute to identify both materials and biological features sustaining the positive impact of graphene on the reduced proliferation of glial cells around the implant to understand the causes (molecular pathway and the dynamics) underlying these effects.

Another aspect that we have investigated is the time robustness of such single monolayer coating once implanted through neural tissues. For that, the conductance of the graphene monolayer wrapping the probes was measured between adjacent electrodes as it provides an accurate in-situ and real-time control of the continuity of the monolayer ($R_{\square}$ = 0.7–1 kΩ $\square^{-1}$). After the surgery (week 1), the measure was repeated giving almost the same value and confirming the presence and the continuity of the monolayer after penetrating the pia matter. However, after the first week, the graphene conductance increases (above the GΩ) for more than half of the coated electrodes, certainly because cells and micromovements of the implant induce few more strains on the graphene monolayer, and contribute further to tear apart the graphene layer along the sharp step at the contact edge (SiO2/IrO*x*) (Figure 4a). But it might also result from a progressive delamination or degradation of graphene by enzymes[50] and by macrophages,[51–53] because of the high intracortical cellular activity (including macrophages) after a blood brain barrier disruption. Nevertheless we consider that if graphene has been degraded, it still played a role during the first weeks after implantation which are well known to be critical in the gliosis process, in particular regarding the massive migration of astrocytes and the regrowth of damaged neurons (e.g., adhesion, neurite spreading, and axonal polarization) that occurs within the first days.[26] Indeed we have observed a significant improvement with graphene coating on the number of working electrodes, i.e., able to detect single spike from isolated motor neurons, which increases by at least two times in comparison with the number of uncoated electrodes. Figure 5c shows also that 100% of coated electrodes are effective for some Gr-coated probe. Moreover, traces of graphene can still be observed after the implants extraction (Figure S5, Supporting Information), although most of the graphene have been teared off during its extraction from the reconstructed tissues. Thus, many scenarios are possible regarding the fate of CVD-grown graphene in vivo, and should require additional investigations such as in-situ or postmortem graphene tracking to follow its possible delamination and the presence of persistent flakes within the tissues.

Finally, graphene can also play the role of a diffusion barrier, preventing toxic release from the probe and acting as a corrosion protection for the metal-based electrodes that could also contribute to reduce the immune reaction.[54,55] Regarding the slow degradation of graphene, the presence of graphene should still prevent the surface ions to diffuse out of the implant during the paroxysm of the inflammation (i.e., during the first week), and thus allow a better healing around the probe. Further experiments conducted over several months, together with real-time and in-situ monitoring of graphene degradation, would provide information on the biodegradation mechanism versus the healing speed at the implant location.

4. Conclusion

We have provided experimental evidences emphasizing the positive impact of graphene within cultured neurons and on the detection efficiency and time reliability of the intracortical implants. The histological analyses show that this improvement is associated with a reduced proliferation of astrocytes and microglia. These results suggest that graphene coating could sustain a healthier neuron network at the implant site and provide the required intimate coupling between the electrode and the target neurons for efficient and chronic recording. Graphene could thus motivate further developments of the graphene neuroelectronics for intracortical interfaces. Because such coating could be implemented on a wide range of substrates, including 3D electrical probes and optical fibers, it could contribute to suppress the rejection of deep-brain interfaces currently used in many research areas, from fundamental neurosciences to medicine. Future work should investigate the time robustness of graphene monolayer coating once implanted through neural tissues, as well as follow the extent and kinetics of its delamination or disruption by neural cells and tissues. Further identification of physiological and material features that sustain the graphene degradation could provide suitable insights for controlling it within neural probes or regenerative scaffolds and pave the way for its use in regenerative medicine.

5. Experimental Section

CVD Graphene Growth and Transfer onto Arbitrary Substrates: Graphene was grown on copper foil (25 µm thick, 99.8% purity, Alfa-Aesar) using CVD as reported earlier,[56] leading to a polycrystalline monolayer with crystal diameter exceeding 20 µm. Prior to the growth, the copper foils were cleaned in acetone and were then annealed in diluted H_2: Ar [1:9] gas at 1000 °C for 2 h. Pieces of Cu foil with graphene layer grown on top were covered with PMMA resist on the graphene side and then wet etched in ammonium persulfate solution (0.1 g mL, 2 h at room temperature). After complete etching of Cu, graphene–PMMA stack was rinsed in several subsequent deionized (DI) water baths. Then the graphene–PMMA film floating on the DI water surface was scooped from below onto a clean substrate and dried at room temperature. Finally, PMMA was removed in an overnight acetone bath followed by the sample thermal annealing for 1 h at 300 °C in vacuum.

Direct Transfer of Monolayer Graphene onto 3D Probes: The PMMA carrier used for transferring graphene on flat substrates appeared to prevent a proper adhesion of the monolayers on intracortical probes, such as Michigan array probe[6] that we used for this study (Figure S4, Supporting Information). A dedicated protocol was then being developed in order to lower the constraints on the graphene layer. Circular pieces of monolayer graphene on copper without PMMA were cut and dropped on a copper fast etchant solution, a 50% diluted Transène PC-100 iron chloride solution for 2 min. The remaining copper was then etched with standard amonium persulfate for 20 min. A syringe was used to slowly rinse out the copper etchant solution five times in a row with DI water. The probes were then cleaned and exposed to oxygen plasma (120 s) to render the surface more hydrophilic. Finally, fast fishing step was done using the tip of the probe—in the middle of the floating graphene sheet—providing a uniform covering of the probe surface. The uniformity and quality of the coating was then assessed by scanning electron microscopy and Raman spectroscopy (Figure 3; Figure S3, Supporting Information).

Cell Culture and Immunofluorescence Imaging: Primary hippocampal neurons were dissociated from E16.5 mouse embryos and seeded with a density of about 120 cells mm^{-2} onto sterilized poly-L-lysine coated chip surface following previously reported culturing protocol.[26] The seeded neurons were incubated at 37 °C and 5% CO_2 in the attachment medium (MEM supplemented with fetal bovine serum) and replaced 3 to 4 h later by glial conditioned neurobasal medium supplemented with AraC (1×10^{-6} M) to stop proliferation of glial cells. Medium was changed once a week. Immunofluorescence staining was performed to assess the neuron density and neurites spreading. For that, neurons were fixed in 4% paraformaldehyde (10 min) and labeled with DAPI, antitau, and antisynapsin primary antibody to visualize the soma, the axon, and synaptic vesicles, respectively.

For cell density counting, somas were detected from optical micrographs with NIH ImageJ software (particle analysis plug-in) after picture down conversion to 8 Bits (grayscale) and threshold definition to extract the background noise. Soma size was first been measured manually on a dozen of neurons per picture in order to define the average soma area to be detected. For groups of cells, each soma cannot be discriminated, thus the number was estimated by dividing the total area of clusters by the average soma size, and then verified with manual counting. The covering rate for each stained surface (total neurite, axon, synapse surfaces) have been extracted with the threshold tool in ImageJ, preserving a constant brightness level for each fluorescent antibody. Defocus—inducing less brightness and larger covering surfaces—was taken into account by keeping the same threshold level of brightness between all pictures.

In-Vivo Assay: Ten adult Thy1-ChR2-YFP transgenic mice were housed individually on 12 h light/dark cycle at 22 ± 1 °C with access to food and water ad libitum. Before surgery, mice were first habituated to human presence and manipulation during 2 weeks. Stereotaxic fixation was performed after administration of 0.1 mL of Dorbene anesthesia and surgeries were performed under anesthesia of 2% diluted isofluorane in 2 L min^{-1} oxygen. Briefly, we used ten Neuronexus Q-trodes probes combining an optical fiber on top of an array of four microelectrodes (recording channels). Five probes were coated with graphene, and five (uncoated) probes were used for control (20 microelectrodes were tested for each condition, i.e., 40 electrodes in total, and on ten independent rodents). Each recording channel are 50 µm wide (diameter) Pt/Ir microelectrode integrated on a 200 µm wide silicon probe (few millimeters long). The probes were inserted within layer V of the right motor cortex, which was previously identified anatomically and electrophysiologically.[41] Signal amplification and recording were made with the Tucker Davis Technologies PZ2 preamp and RZ2 amplifier at the sampling frequency of 25 kHz. Spikes are sorted using principal component analysis in real-time with TdT OpenEx Synapse software and spikes of interest were selected when spike occurrence was synchronized with the walk. Each electrode that could detect one or more motoneurons signal have been tracked by repeating the experiment once a week with in-cage free-movement recordings for all sensors and compared to previous results.

Histology: At the end of the experimental procedures, mice were perfused with Ringer's solution containing 100 000 IU L^{-1} heparin and 0.25% $NaNO_2$ followed by 4% phosphate buffered paraformaldehyde,

pH 7.4 containing 5% sucrose. The brains were extracted, postfixed overnight, and transferred to 30% phosphate-buffered sucrose for cryoprotection. After 4 d, the tissue was embedded and the brains sectioned in a cryostat (Leica, Germany) at a 40 µm thickness. Astrocytic and microglial reactivity was revealed with immunohistological staining against glial fibrillary acidic protein (GFAP) and ionized calcium binding adapter molecule 1 (Iba1), respectively. Briefly, the brain sections were incubated overnight with the anti-Iba1 (1:1000, Abcam) or anti-GFAP (1:1000, Dako) primary antibodies. Fluorescence counterstaining of Nissl substance was done using neurotrace 640/660 solution (1:50, Invitrogen). The brain slices were then observed with a laser confocal fluorescence microscope (Leica SPE, Germany) to estimate the population of both neuron and glial cells and its density around the implanted probes. Immunostaining density was measured offline using representative confocal images of motor cortex sections. Images were acquired using standard imaging settings that were kept constant across all test animals.

Supporting Information

Supporting Information is available from the Wiley Online Library or from the author.

Acknowledgements

Animal care and experiments have been conducted in accordance with standard ethical European Committee Guidelines on the Care and Use of Laboratory Animals. All procedures have been submitted for approval to local ethics committees (University Grenoble-Alpes or Veterinarian Office Vaud, Switzerland). Experiments have been performed in an authorized establishment under the supervision of authorized investigators. The authors gratefully acknowledge financial support from la Région Rhône-Alpes (COOPERA project) and from the french Agence Nationale de la Recherche under the projects ANR-18-CE42-0003-01 (NanoMesh) and ANR-10-LABX-51-01 (Labex LANEF du Programme d'Investissements d'Avenir, the Lab Alliances on Nanosciences – Energies for the Future and the EU Graphene Flagship.

Conflict of Interest

The authors declare no conflict of interest.

Keywords

biomaterials, brain interface, chronic recordings, graphene, surface functionalization

Received: October 21, 2018
Revised: July 16, 2019
Published online:

[1] J. L. Collinger, B. Wodlinger, J. E. Downey, W. Wang, E. C. Tyler-Kabara, D. J. Weber, A. J. McMorland, M. Velliste, M. L. Boninger, A. B. Schwartz, *Lancet* **2013**, *381*, 557.
[2] D. M. Taylor, S. I. H. Tillery, A. B. Schwartz, *Science* **2002**, *296*, 1829.
[3] M. D. Serruya, N. G. Hatsopoulos, L. Paninski, M. R. Fellows, J. P. Donoghue, *Nature* **2002**, *416*, 141.
[4] M. Bonizzato, G. Pidpruzhnykova, J. DiGiovanna, P. Shkorbatova, N. Pavlova, S. Micera, G. Courtine, *Nat. Commun.* **2018**, *9*, 3015.
[5] P. K. Campbell, K. E. Jones, R. J. Huber, K. W. Horch, R. A. Normann, *IEEE Trans. Biomed. Eng.* **1991**, *38*, 758.
[6] D. R. Kipke, R. J. Vetter, J. C. Williams, J. F. Hetke, *IEEE Trans. Neural Syst. Rehabil. Eng.* **2003**, *11*, 151.
[7] U. Chaudhary, N. Birbaumer, A. Ramos-Murguialday, *Nat. Rev. Neurol.* **2016**, *12*, 513.
[8] L. R. Hochberg, D. Bacher, B. Jarosiewicz, N. Y. Masse, J. D. Simeral, J. Vogel, S. Haddadin, J. Liu, S. S. Cash, P. van der Smagt, J. P. Donoghue, *Nature* **2012**, *485*, 372.
[9] L. R. Hochberg, M. D. Serruya, G. M. Friehs, J. A. Mukand, M. Saleh, A. H. Caplan, A. Branner, D. Chen, R. D. Penn, J. P. Donoghue, *Nature* **2006**, *442*, 164.
[10] R. Biran, D. C. Martin, P. A. Tresco, *Exp. Neurol.* **2005**, *195*, 115.
[11] A. Prasad, Q.-S. Xue, R. Dieme, V. Sankar, R. Mayrand, T. Nishida, W. J. Streit, J. C. Sanchez, *Front. Neuroeng.* **2014**, *7*, 2.
[12] M. Jorfi, J. L. Skousen, C. Weder, J. R. Capadona, *J. Neural Eng.* **2015**, *12*, 011001.
[13] S. P. Lacour, G. Courtine, J. Guck, *Nat. Rev. Mater.* **2016**, *1*, 16063.
[14] C. Im, J.-M. Seo, *Biomed. Eng. Lett.* **2016**, *6*, 104.
[15] S. P. Lacour, S. Benmerah, E. Tarte, J. FitzGerald, J. Serra, S. McMahon, J. Fawcett, O. Graudejus, Z. Yu, B. Morrison, *Med. Biol. Eng. Comput.* **2010**, *48*, 945.
[16] D.-H. Kim, J. Viventi, J. J. Amsden, J. Xiao, L. Vigeland, Y.-S. Kim, J. A. Blanco, B. Panilaitis, E. S. Frechette, D. Contreras, D. L. Kaplan, F. G. Omenetto, Y. Huang, K. C. Hwang, M. R. Zakin, B. Litt, J. A. Rogers, *Nat. Mater.* **2010**, *9*, 511.
[17] S. M. Wellman, J. R. Eles, K. A. Ludwig, J. P. Seymour, N. J. Michelson, W. E. McFadden, A. L. Vazquez, T. D. Kozai, *Adv. Funct. Mater.* **2018**, *28*, 1701269.
[18] I. R. Minev, P. Musienko, A. Hirsch, Q. Barraud, N. Wenger, E. M. Moraud, J. Gandar, M. Capogrosso, T. Milekovic, L. Asboth, R. F. Torres, N. Vachicouras, Q. Liu, N. Pavlova, S. Duis, A. Larmagnac, J. Vörös, S. Micera, Z. Suo, G. Courtine, S. P. Lacour, *Science* **2015**, *347*, 159.
[19] S. Park, Y. Guo, X. Jia, H. K. Choe, B. Grena, J. Kang, J. Park, C. Lu, A. Canales, R. Chen, Y. S. Yim, G. B. Choi, Y. Fink, P. Anikeeva, *Nat. Neurosci.* **2017**, *20*, 612.
[20] Y. Lu, H. Lyu, A. G. Richardson, T. H. Lucas, D. Kuzum, *Sci. Rep.* **2016**, *6*, 33526.
[21] D.-W. Park, A. A. Schendel, S. Mikael, S. K. Brodnick, T. J. Richner, J. P. Ness, M. R. Hayat, F. Atry, S. T. Frye, R. Pashaie, S. Thongpang, Z. Ma, J. C. Williams, *Nat. Commun.* **2014**, *5*, 5258.
[22] B. M. Blaschke, N. Tort-Colet, A. Guimerà-Brunet, J. Weinert, L. Rousseau, A. Heimann, S. Drieschner, O. Kempski, R. Villa, M. V. Sanchez-Vives, J. A. Garrido, *2D Mater.* **2017**, *4*, 025040.
[23] A. Bendali, L. H. Hess, M. Seifert, V. Forster, A.-F. Stephan, J. A. Garrido, S. Picaud, *Adv. Healthcare Mater.* **2013**, *2*, 929.
[24] N. Li, X. Zhang, Q. Song, R. Su, Q. Zhang, T. Kong, L. Liu, G. Jin, M. Tang, G. Cheng, *Biomaterials* **2011**, *32*, 9374.
[25] J. S. Lee, A. Lipatov, L. Ha, M. Shekhirev, M. N. Andalib, A. Sinitskii, J. Y. Lim, *Biochem. Biophys. Res. Commun.* **2015**, *460*, 267.
[26] F. Veliev, A. Briançon-Marjollet, V. Bouchiat, C. Delacour, *Biomaterials* **2016**, *86*, 33.27.
[27] S. Y. Park, J. Park, S. H. Sim, M. G. Sung, K. S. Kim, B. H. Hong, S. Hong, *Adv. Mater.* **2011**, *23*, H263.
[28] J. Kim, S. Park, Y. J. Kim, C. S. Jeon, K. T. Lim, H. Seonwoo, S.-P. Cho, T.D. Chung, P.-H. Choung, Y.-H. Choung, B.H. Hong, J.H. Chung, *J. Biomed. Nanotechnol.* **2015**, *11*, 2024.
[29] L. Karumbaiah, T. Saxena, D. Carlson, K. Patil, R. Patkar, E. A. Gaupp, M. Betancur, G.B. Stanley, L. Carin, R. V. Bellamkonda, *Biomaterials* **2013**, *34*, 8061.
[30] T. D. Kozai, Z. Du, Z. V. Gugel, M. A. Smith, S. M. Chase, L. M. Bodily, E.M. Caparosa, R.M. Friedlander, X. T. Cui, *J. Neurosci. Methods* **2015**, *242*, 15.

[31] J. C. Barrese, N. Rao, K. Paroo, C. Triebwasser, C. Vargas-Irwin, L. Franquemont, J. P. Donoghue, *J. Neural Eng.* **2013**, *10*, 066014.
[32] L. A. Flanagan, Y. E. Ju, B. Marg, M. Osterfield, P. A. Janmey, *NeuroReport* **2002**, *13*, 2411.
[33] M. Tessier-Lavigne, C. S. Goodman, *Science* **1996**, *274*, 1123.
[34] K. Franze, J. Gerdelmann, M. Weick, T. Betz, S. Pawlizak, M. Lakadamyali, J. Bayer, K. Rillich, M. Gogler, A. Reichenbach, P. Janmey, J. Kas, *Biophys. J.* **2009**, *97*, 1883.
[35] R. J. Edgington, A. Thalhammer, J. O. Welch, A. Bongrain, P. Bergonzo, E. Scorsone, R. B. Jackman, R. Schoepfer, *J. Neural Eng.* **2013**, *10*, 056022.
[36] J. L. Wierman, J. S. Alden, C. U. Kim, P. L. McEuen, S. M. Gruner, *J. Appl. Crystallogr.* **2013**, *46*, 1501.
[37] M. K. Blees, A. W. Barnard, P. A. Rose, S. P. Roberts, K. L. McGill, P. Y. Huang, A. R. Ruyack, J. W. Kevek, B. Kobrin, D. A. Muller, P. L. McEuen, *Nature* **2015**, *524*, 204.
[38] D. Graf, F. Molitor, K. Ensslin, C. Stampfer, A. Jungen, C. Hierold, L. Wirtz, *Nano Lett.* **2007**, *7*, 238.
[39] F. Veliev, Z. Han, D. Kalita, A. Briançon-Marjollet, V. Bouchiat, C. Delacour, *Front. Neurosci.* **2017**, *11*, 466.
[40] S. Gawad, M. Giugliano, M. O. Heuschkel, B. Wessling, H. Markram, U. Schnakenberg, P. Renaud, H. Morgan, *Front. Neuroeng.* **2009**, *2*, 1.
[41] J. DiGiovanna, N. Dominici, L. Friedli, J. Rigosa, S. Duis, J. Kreider, J. Beauparlant, R. van den Brand, M. Schieppati, S. Micera, G. Courtine, *J. Neurosci.* **2016**, *36*, 10440.
[42] N. Li, T. W. Chen, Z. V. Guo, C. R. Gerfen, K. Svoboda, *Nature* **2015**, *519*, 51.
[43] J. W. Salatino, K. A. Ludwig, T. D. Kozai, E. K. Purcell, *Nat. Biomed. Eng.* **2017**, *1*, 862.
[44] J. Groothuis, N. F. Ramsey, G. M. Ramakers, G. van der Plasse, *Brain Stimul.* **2014**, *7*, 1.
[45] M. Okun, A. Lak, M. Carandini, K. D. Harris, *PLoS One* **2016**, *11*, e0151180.
[46] N. Arimura, K. Kaibuchi, *Nat. Rev. Neurosci.* **2007**, *8*, 194.
[47] E. K. F. Yim, S. W. Pang, K. W. Leong, *Exp. Cell Res.* **2007**, *313*, 1820.
[48] K. Franze, J. Gerdelmann, M. Weick, T. Betz, S. Pawlizak, M. Lakadamyali, J. Bayer, K. Rillich, M. Gögler, Y.-B. Lu, A. Reichenbach, P. Janmey, J. Käs, *Biophys. J.* **2009**, *97*, 1883.
[49] M. Bramini, G. Alberini, E. Colombo, M. Chiacchiaretta, M. L. DiFrancesco, J. F. Maya-Vetencourt, L. Maragliano, F. Benfenati1, F. Cesca, *Front. Syst. Neurosci.* **2018**, *12*, 12.
[50] G. P. Kotchey, Y. Zhao, V. E. Kagan, A. Star, *Adv. Drug Delivery Rev.* **2013**, *65*, 1921.
[51] Y. Sato, A. Yokoyama, Y. Nodasaka, T. Kohgo, K. Motomiya, H. Matsumoto, E. Nakazawa, T. Numata, M. Zhang, M. Yudasaka, H. Hara, R. Araki, O. Tsukamoto, H. Saito, T. Kamino, F. Watari, K. Tohji, *Sci. Rep.* **2013**, *3*, 2516.
[52] C. M. Girish, A. Sasidharan, G. S. Gowd, S. Nair, M. Koyakutty, *Adv. Healthcare Mater.* **2013**, *2*, 1489.
[53] A. Nunes, C. Bussy, L. Gherardini, M. Meneghetti, M. A. Herrero, A. Bianco, M. Prato, T. Pizzorusso, K. T. Al-Jamal, K. Kostarelos, *Nanomedicine* **2012**, *7*, 1485.
[54] A. Krishnamurthy, V. Gadhamshetty, R. Mukherjee, Z. Chen, W. Ren, H. M. Cheng, N. Koratkar, *Carbon* **2013**, *56*, 45.
[55] A. Krishnamurthy, V. Gadhamshetty, R. Mukherjee, B. Natarajan, O. Eksik, S. A. Shojaee, D.A. Lucca, W. Ren, N. Hui-Ming Cheng Koratkar, *Sci. Rep.* **2015**, *5*, 13858.
[56] Z. Han, A. Kimouche, D. Kalita, A. Allain, H. Arjmandi-Tash, A. Reserbat-Plantey, L. Marty, S. Pairis, V. Reita, N. Bendiab, J. Coraux, V. Bouchiat, *Adv. Funct. Mater.* **2014**, *24*, 6412.